Response to Reviewers' Comments

Reviewer #2:

'Comment on egusphere-2026-1091'

General Comments

This paper uses one year of observations from a newly established national Ka-band cloud radar network to characterize cloud vertical structure across China, including cloud occurrence, layer number, CBH, CTH, and CT, and further relates these properties to humidity, lower-tropospheric stability, wind shear, and land cover. The dataset is clearly valuable, especially because the 1-min temporal resolution and 30-m vertical resolution allow the authors to examine seasonal and diurnal variations that are difficult to resolve from satellites or radiosondes. The paper's main contribution is therefore not only the national-scale description of cloud vertical structure, but also the attempt to connect these observed structures with thermodynamic, dynamical, and land-surface controls. Overall, the study has strong observational potential and could provide useful benchmarks for model evaluation, but several issues need to be addressed before the physical conclusions can be considered fully convincing.

Response: We thank the reviewer for his/her comprehensive evaluation and thoughtful comments, which help tremendously to improve the quality of our work. We have tried our best to address the reviewer's concerns one by one.

Per your kind suggestions, substantial changes have been made, including adding more critical references on the topic analyzed here, complementing the lower-tropospheric stability (a metric for atmospheric stability), streamlining the text, more in-depth discussion and result interpretation, among others. For more details, please refer to the revised manuscript.

For clarity purpose, here we have listed the reviewer's comments in black, followed by our responses in blue, and the modifications to the manuscript are in italics. We sincerely hope that the reply and the revisions can satisfy the reviewer's expectations.

Specific Comments:

1.One limitation is the short time period. All major statistics are based on 2024, but the manuscript often presents the results as a national-scale benchmark. Cloud vertical structure over China can be strongly affected by monsoon variability, large-scale circulation anomalies, regional drought or wet conditions, and unusual synoptic patterns in a given year. The authors may discuss how representative 2024 is, for example by comparing cloud fraction, precipitation, humidity, stability, or circulation conditions with multi-year satellite or reanalysis records.

Response: We sincerely thank the reviewer for raising this insightful and critical comment regarding the representativeness of our single-year dataset. We fully agree that a single year of observations cannot constitute long-term climatology, and we have addressed this concern from three perspectives: (i) justification for selecting 2024, (ii) a quantitative representativeness assessment using ERA5 reanalysis, and (iii) tempered language throughout the revised manuscript.

(1) Why 2024 was selected

Prior to 2024, fewer than 30 MMCRs were operational across China, which was insufficient for reliable national-scale analysis of cloud vertical structure (CVS). In 2024, the network underwent a major expansion to nearly 120 stations, of which 80 met our strict data-quality criterion (≥100 valid observation days per year, defined as calendar days with at least 8 hours of valid MMCR measurements). Thus, 2024 represents the first year in which a sufficiently dense observing network became available, making it the only feasible foundation for this pioneering investigation. This justification has been added to Section 2.1.1 of the revised manuscript, as follows:

"MMCR data have been widely used in cloud boundary detection (e.g., Zhang et al., 2017; Zhou et al., 2019; Fang et al., 2023) and exhibit strong consistency with radiosonde observations (Wang et al., 2016; Zhao et al., 2017; Chen et al., 2022). In this study, MMCR data for the year of 2024 were obtained from the China Meteorological Administration (CMA). Of the 120 MMCR stations operating across China in 2024, only those with at least 100 valid observation days annually (*defined as calendar days with at least 8 hours of valid MMCR measurements*) were retained to ensure data quality. This criterion resulted in the selection of 80 stations for subsequent analysis (Fig. 1). *Notably, we selected 2024 because it was the first year in which the MMCR network achieved sufficient density for national-scale analysis. Before 2024, fewer than 30 stations were operational nationwide, which was inadequate for a robust spatial characterization of CVS. The major expansion in 2024, with nearly 120 MMCRs deployed, made this pioneering investigation feasible. Even though this single-year dataset does not constitute a long-term climatology, it provides the first observationally dense and vertically resolved national snapshot of CVS across China.* "

(2) Representativeness of 2024 relative to the past decade

Following the reviewer's suggestion, we evaluated the representativeness evaluation of 2024 using ERA5 reanalysis data for 2014 to 2023 as the climatological baseline. We calculated standardized anomalies (Z-scores) of annual mean total cloud cover, precipitation, and 2 m specific humidity (q_{2m}) in 2024. A Z-score within ± 2 is generally considered to reflect typical interannual variability. The key results are summarized in Figure R1 (provided below for the reviewer's reference only), as follows,

Total cloud cover: The ERA5-derived annual mean cloud cover for 2024 is 54.54%, nearly identical to the 2014–2023 climatological mean of 54.05% (relative deviation 0.9%, Z-score well below 1.0). This indicates that the overall cloud cover in 2024 falls well within the range of natural interannual variability, and that our MMCR-derived cloud occurrence statistics are not unduly influenced by anomalous cloud cover. This supports the reliability of the CVS metrics (CBH, CTH, CT) derived from the 2024 observations.

Precipitation: The Z-score for annual mean precipitation in 2024 is 1.8, indicating a notably wetter-than-normal year.

Low-level moisture: 2024 shows a pronounced positive anomaly in q_{2m}, with a Z-score of 3.5, representing an exceptionally high value relative to the past decade.

Rather than undermining our conclusions, these anomalous moisture and precipitation conditions provide a valuable "natural experiment" that reinforces the physical mechanisms proposed in our study. As we demonstrate in Section 3.5, enhanced low-level moisture promotes deeper vertical cloud development. The anomalously high precipitation in 2024 is consistent with this enhanced moisture-driven convection, and it aligns with our observed elevated cloud top heights and cloud thickness under humid conditions. In other words, 2024 exhibited near-normal cloud frequency but extreme low-level moisture—exactly the combination that our core argument predicts: moisture availability primarily controls the vertical extent of clouds once they form, rather than their occurrence frequency. Therefore, the CVS–thermodynamic relationships we derive are not artifacts of an anomalous year; rather, they are physically consistent and likely conservative relative to drier years.

We acknowledge that the single-year nature of the dataset precludes definitive multi-year climatological conclusions. We have therefore adopted a cautious tone throughout the manuscript, replacing absolute statements with precise wording such as "first observational assessment for 2024" and "an unprecedented snapshot." In the Abstract and Conclusions, we explicitly state that this record provides a baseline for future multi-year evaluations rather than long-term climatology.

(3) Specific textual revisions

We have revised the Abstract as follows:

"Using a newly established national network of 80 Ka-band millimeter-wave cloud radars (MMCRs), *here we present a high-spatiotemporal-resolution (vertical resolution of 30 m, temporal resolution of 1 min) characterization of CVS across China based on one year (2024) of observations*, and quantify its thermodynamic, dynamical, and land-surface controls. "

In the Summary and Conclusions, we now state:

"This study presents the first national-scale, high-spatiotemporal-resolution *analysis* of CVS across China based on observations from a coordinated network of 80 Ka-band cloud radars *during 2024, providing an unprecedentedly detailed snapshot (30 m vertical, 1 min temporal resolution) of cloud vertical structures and their governing factors*."

"Overall, this study provides a high-resolution, observationally constrained snapshot of cloud vertical structure across China and establishes a quantitative framework linking CVS metrics to thermodynamic, dynamical, and land-surface controls (Figure 15). ... *Although this one-year record does not support long-term trend analysis, it establishes a robust baseline against which model-simulated CVS can be evaluated across timescales, especially when combined with multi-year satellite or reanalysis products, thereby supporting iterative improvement of cloud schemes and enhancing prediction skill from weather to climate scales. Future work should extend this analysis to multi-year datasets to assess interannual variability and explore the role of CVS in extreme weather events and regional climate feedbacks.* "

We believe these revisions and the accompanying analysis adequately address the Reviewer's concern. We are grateful for the suggestion, which has significantly strengthened the manuscript.

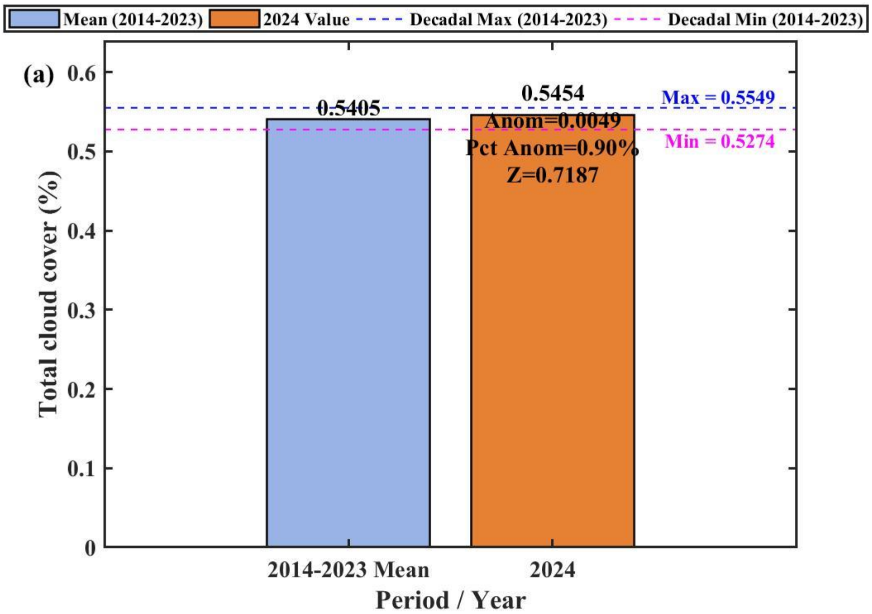

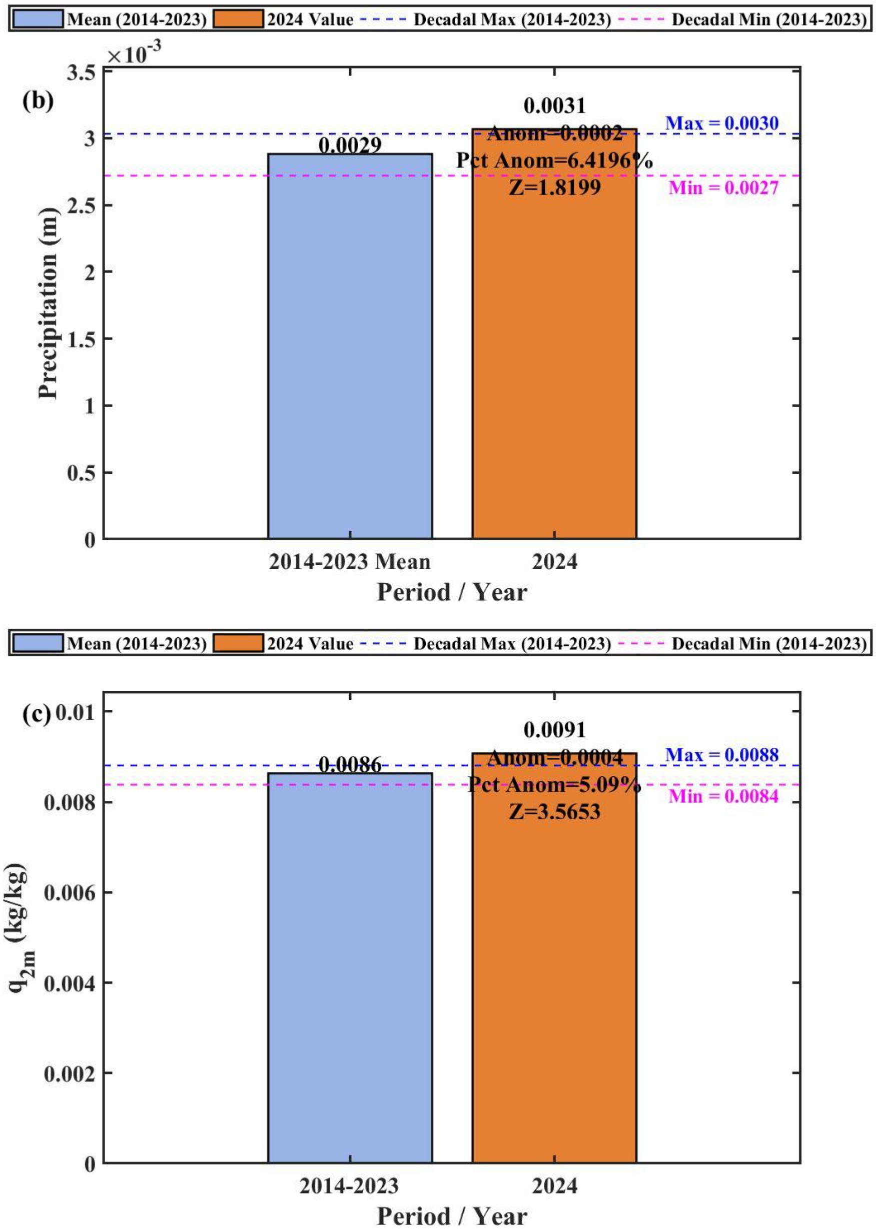

Figure R1. Comparison of the annual mean (a) total cloud cover (%), (b) precipitation (m), and (c) 2 m specific humidity (kg kg^{-1}; q_{2m}) over China between the 2014–2023 decadal mean (blue bars) and the year 2024 (orange bars). In each subfigure, the dashed horizontal lines represent the decadal maximum (blue) and minimum (magenta) over the 2014–2023 period. Numerical values are displayed on or with the bars; for 2024, the label additionally includes the absolute anomaly (2024 minus decadal mean), the percentage anomaly relative to the decadal mean, and the standardized anomaly (Z-score, normalized by the decadal standard deviation). The legend shown at the top applies to all three panels.

2.The retrieval algorithm may need more validation. The height-dependent sensitivity threshold and clutter-removal method are reasonable, but the final cloud occurrence, layer number, CBH, CTH, and CT depend on several empirical thresholds, including the variance criteria, the −20 dBZ filter, and the thin-layer merging/removal rules. These choices may affect thin clouds, weak high clouds, multilayer clouds, and precipitation-contaminated cases. Is it possible to include systematic validation against independent observations, such as ceilometer, radiosonde-derived cloud layers, lidar, or active satellite products?

Response: We sincerely thank the reviewer for this critical and constructive comment. We fully agree that validation against independent observations is essential to verify the reliability of our improved CVS retrieval algorithm, especially given the multiple empirical thresholds adopted in our algorithm.

To address this concern, we have conducted case-based validation using independent radiosonde observations, focusing on the challenging cloud types prone to retrieval uncertainties, including low-level thin cloud, thin mid-level cloud, thick high-level cloud, multi-layer cloud, and deep precipitating cloud. We selected six representative cases covering these categories.

For each of the six cases, we constructed standardized three-panel comparative plots and integrated them into a unified supplementary figure (Fig. S2). The left panel shows the statistical distribution of 30-minute MMCR reflectivity samples, overlaid with three height-dependent detection thresholds (S0, S1, S2) for signal reliability validation. The middle panel presents the 30-minute time-height cross-section of MMCR radar reflectivity, with markers indicating our retrieved CBH and CTH. The right panel illustrates cloud layers diagnosed from collocated radiosonde profiles using the relative-humidity-gradient method proposed by Xu et al. (2023), with green shading denoting the identified cloud boundaries.

The detailed validation results are summarized as follows:

Case 1 (low-level thin cloud): Panels a1 and b1 show a distinct single-layer boundary-layer cloud situated at an altitude of roughly 500 m, with a vertical extent of only 200–300 m. Our variance-based ground clutter suppression effectively isolates this shallow cloud signal from low-level ground interference (b1). The CBH and CTH retrieved from MMCR match the near-surface saturated humidity layer diagnosed by collocated radiosonde profiles (c1), with nearly negligible vertical offsets between radar and radiosonde cloud boundaries. This close agreement validates the effectiveness of our variance-based criteria for distinguishing true cloud echoes from ground clutter.

Case 2 (mid-level thin cloud): This single-layer cloud continuously occupies the 4–6 km altitude range with weak-to-moderate radar reflectivity (a2, b2). The height-dependent thresholds, combined with a -20 dBZ minimum reflectivity cutoff, effectively isolate these faint mid-level cloud echoes from background noise. The excellent agreement between MMCR-retrieved cloud boundaries (CBH/CTH) and radiosonde-derived cloud boundaries, with nearly negligible vertical offsets (c2), confirms that this cutoff reliably retains true cloud signals while excluding noise.

Case 3 (high-level thick cloud): This single-layer cloud extends from roughly 9 to 12 km with relatively weak-to-moderate reflectivity (a3, b3). After variance-based clutter suppression removes spurious low-level noise (4–6 km), the -20 dBZ reflectivity threshold is applied to isolate genuine cloud signals. The resulting MMCR-retrieved CBH and CTH align closely with the radiosonde-diagnosed saturated upper-tropospheric humidity band, with vertical offsets consistently within 0.5 km (c3), which further confirms that the -20 dBZ threshold effectively filters out noise without erroneously removing authentic cloud signals.

Case 4 (multi-layer cloud, first scenario): This case consists of vertically overlapping mid-level cloud echoes characterized by extensive moderate-to-strong radar reflectivity signals (panels a4, b4). The combination of height-dependent sensitivity thresholds and variance-based ground clutter filtering reliably isolates genuine cloud echoes from low-altitude ground interference and instrumental background noise. The time–height cross-section (b4) reveals that the cloud vertical structure evolves rapidly over the half-hour observation window, with the number of distinct cloud decks varying from one to three layers. Our algorithm accurately tracks these individual cloud layers during their formation, merging and dissipation processes, and marks the CBH and CTH of each layer with dedicated symbols, which validates the robustness of our rules for thin-cloud merging and elimination. In comparison, the radiosonde humidity profile (green shaded saturated region in c4) only provides a single instantaneous snapshot and fails to capture such temporal variability; it merely presents a unified continuous saturated layer that integrates all vertically separated cloud decks.

Case 5 (multi-layer cloud, second scenario): This analogous multi-layer case (panels a5, b5, c5) further validates the robustness of our retrieval scheme under complex multi-layer conditions. As in Case 4, our algorithm successfully resolves vertically stacked thin-to-moderate cloud layers, avoids false detection amid overlapping echoes.

Case 6 (deep precipitating cloud): This case features a deep precipitating cloud extending from near-surface to ~11 km with strong reflectivity (a6, b6). Height-dependent thresholds and variance-based clutter filtering reliably separate cloud and precipitation signals from ground interference, and the algorithm correctly identifies the continuous cloud boundaries (CBH/CTH) throughout the observation period. The collocated radiosonde profile (c6) shows a deep saturated layer, which matches the MMCR-retrieved cloud extent closely, with only minor vertical differences (within 1 km). This confirms that the retrieval framework remains robust and produces credible cloud boundaries even for deep, heavily precipitating systems.

Across all six validation cases, the consistent agreement between MMCR retrievals and radiosonde-derived cloud layers demonstrates that our radar-retrieved CBH, CTH, and layer number are in good agreement with independent observations. For thin and weak clouds, the height-dependent sensitivity threshold successfully distinguishes authentic cloud echoes from instrumental noise. Minor mismatches between MMCR and radiosonde cloud retrievals are physically reasonable, primarily arising from temporal sampling mismatch: the MMCR operates at 1-min temporal resolution, whereas radiosondes are launched only twice daily.

We have added a summary of this validation exercise in Section 2.3 (CVS retrieval methods) and supplemented the new figure (Fig. S2) with a detailed descriptive caption in the supplementary materials. The revised manuscript text is presented as follows:

"To evaluate the performance of our improved retrieval algorithm for various cloud categories (including low-level thin cloud, mid-level thin cloud, high-level thick cloud, multi-layer cloud, and deep precipitating cloud), we conducted case-based validation against collocated radiosonde observations (Fig. S2). Comparisons reveal good agreement between radar-retrieved cloud boundaries and cloud limits derived from radiosonde profiles processed following the algorithm proposed by Xu et al. (2023). Vertical discrepancies of CBH and CTH are nearly negligible for thin low-level and mid-level clouds, constrained within 0.5 km for thick high-level clouds, and limited to 1 km for precipitating cloud systems."

We hope this newly added validation analysis greatly strengthens the reliability assessment of our CVS retrieval scheme and fully resolves the reviewer's concern. We again appreciate this insightful suggestion, which has markedly elevated the quality of this manuscript.

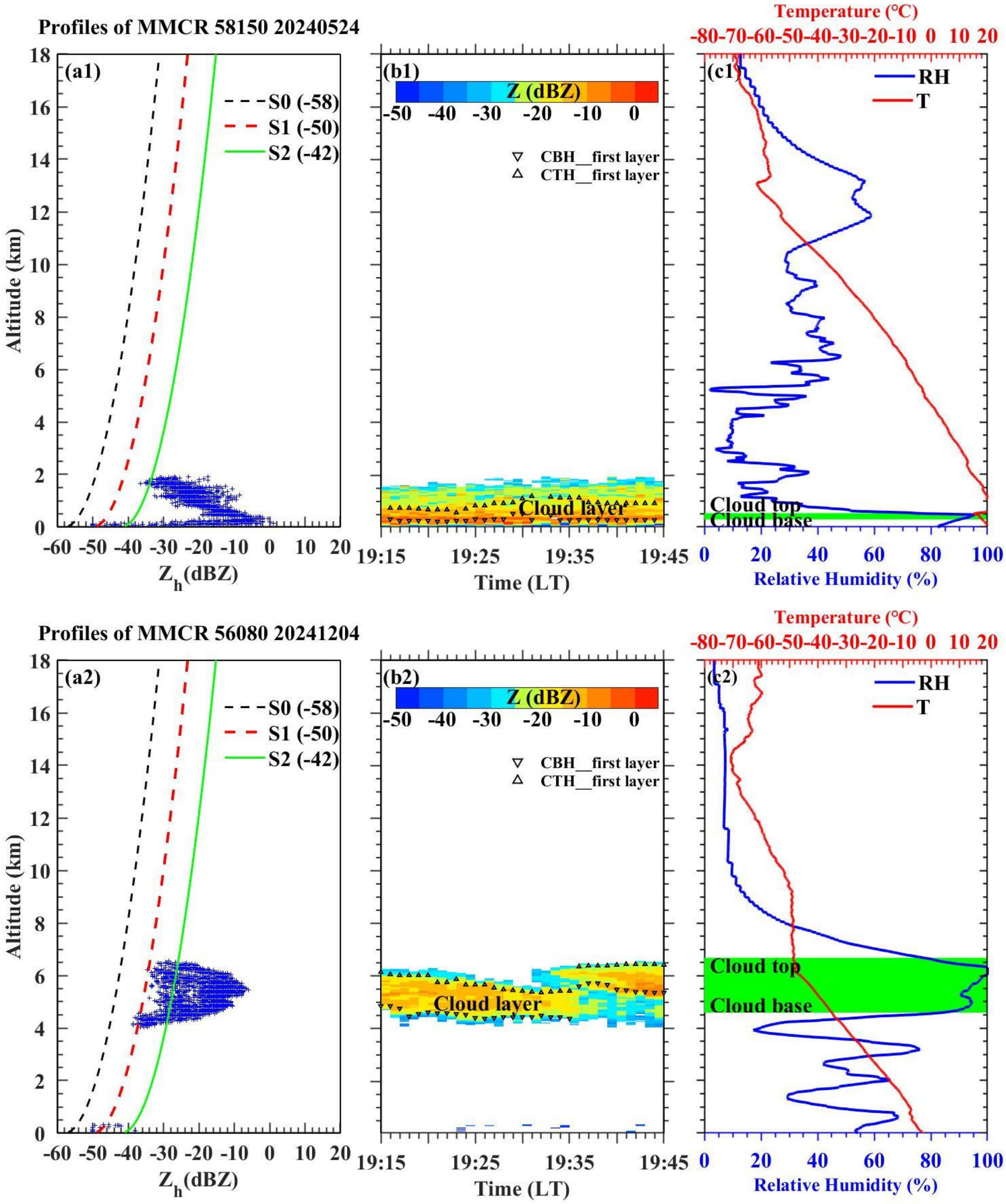

Profiles of MMCR 58150 20240524
(a1)
S0 (-58)
S1 (-50)
S2 (-42)
Altitude (km)
Z_h(dBZ)
(b1)
Z (dBZ)
CBH__first layer
CTH__first layer
Cloud layer
Time (LT)
Temperature (°C)
(c1)
RH
T
Cloud top
Cloud base
Relative Humidity (%)
Profiles of MMCR 56080 20241204
(a2)
S0 (-58)
S1 (-50)
S2 (-42)
Altitude (km)
Z_h(dBZ)
(b2)
Z (dBZ)
CBH__first layer
CTH__first layer
Cloud layer
Time (LT)
Temperature (°C)
(c2)
RH
T
Cloud top
Cloud base
Relative Humidity (%)

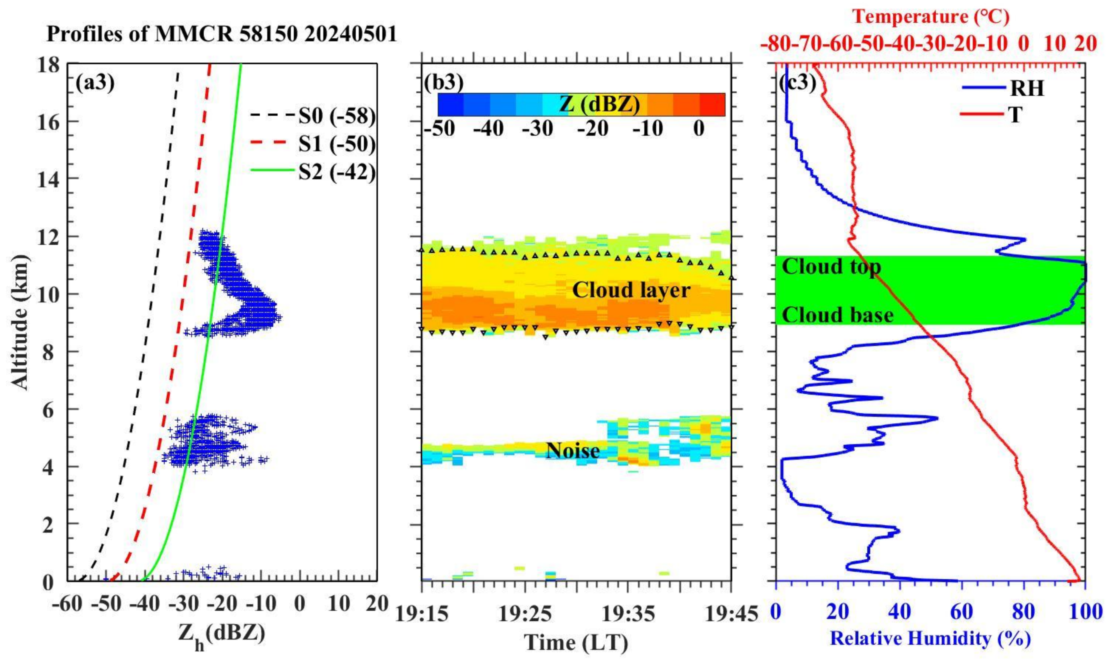
Profiles of MMCR 58150 20240501
(a3)
S0 (-58)
S1 (-50)
S2 (-42)
Altitude (km)
Z_h(dBZ)
(b3)
Z (dBZ)
Cloud layer
Noise
Time (LT)
(c3)
Temperature (°C)
RH
T
Cloud top
Cloud base
Relative Humidity (%)

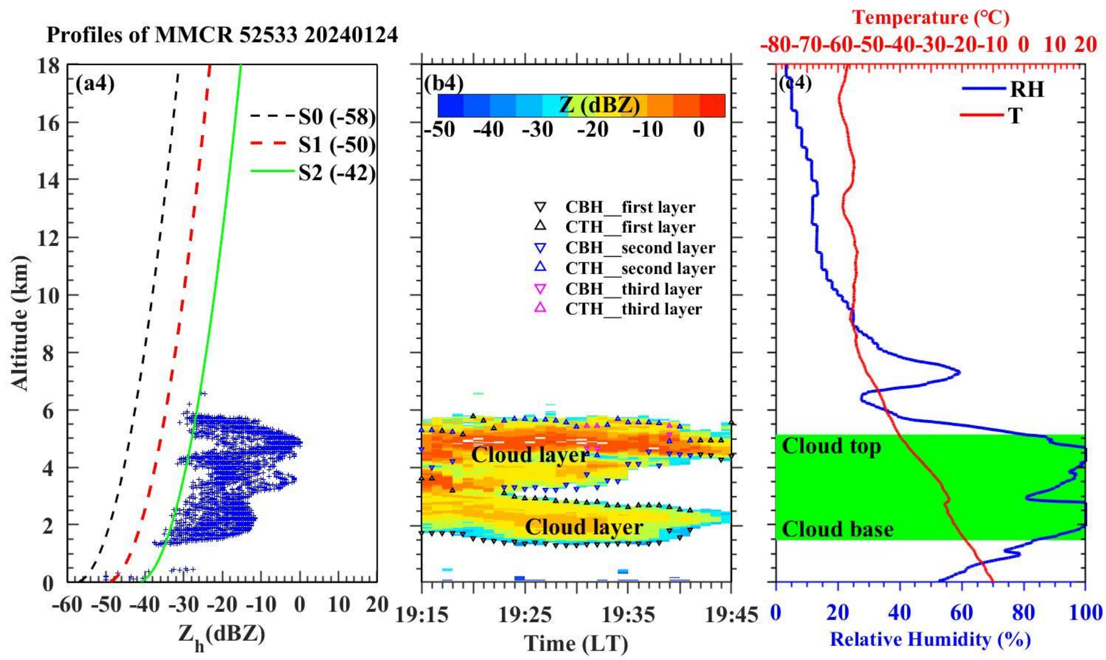
Profiles of MMCR 52533 20240124
(a4)
S0 (-58)
S1 (-50)
S2 (-42)
Altitude (km)
Z_h(dBZ)
(b4)
Z (dBZ)
CBH__first layer
CTH__first layer
CBH__second layer
CTH__second layer
CBH__third layer
CTH__third layer
Cloud layer
Cloud layer
Time (LT)
(c4)
Temperature (°C)
RH
T
Cloud top
Cloud base
Relative Humidity (%)

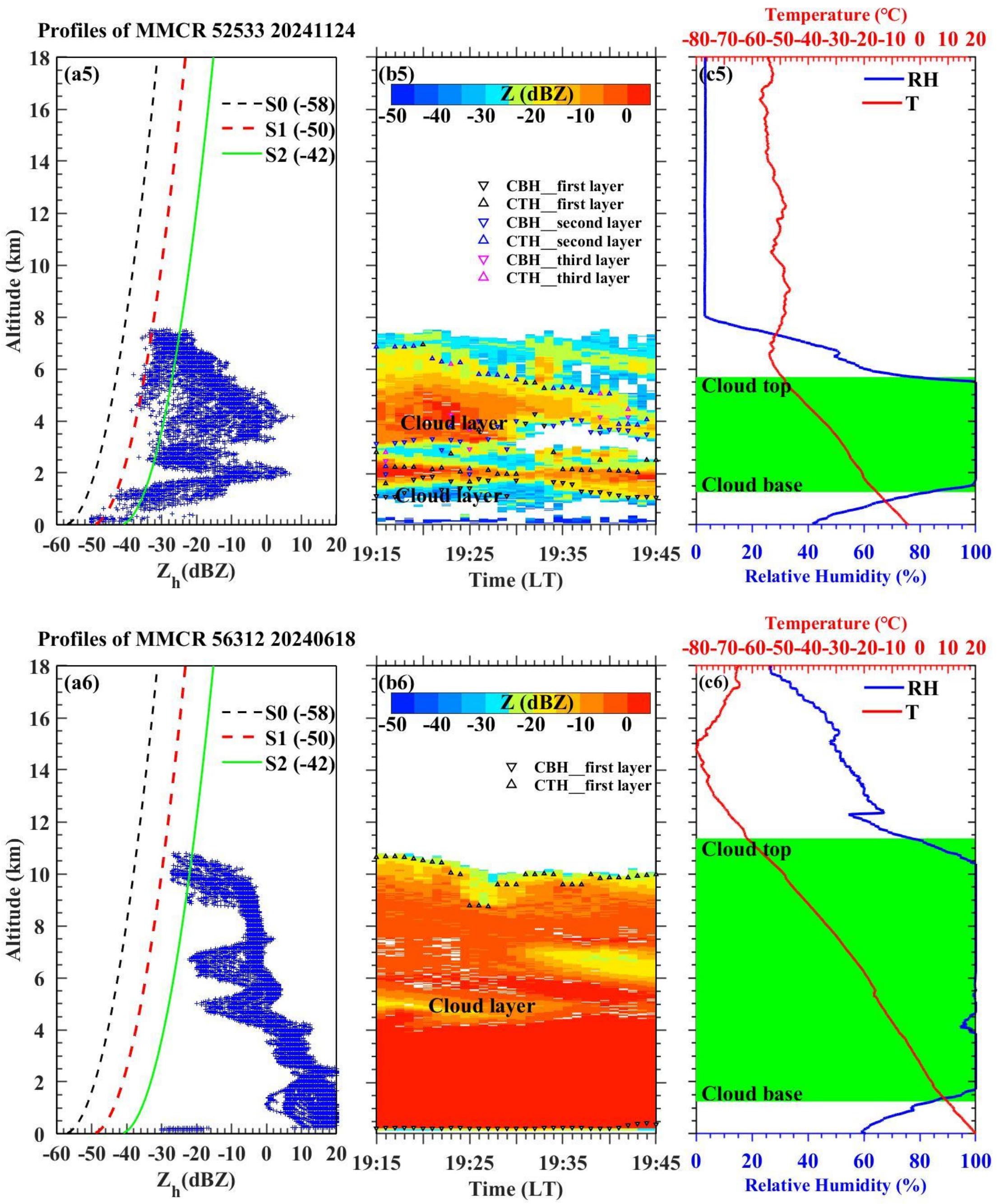

Figure S2. Comparison of six representative cases between MMCR-retrieved cloud vertical structure and collocated radiosonde cloud layers. The first column of panels shows height-dependent detection thresholds S0, S1, and S2 (with their respective threshold values indicated in brackets) overlaid with instantaneous radar reflectivity samples. The middle column presents time-height cross-sections of MMCR reflectivity factor Z (dBZ), with inverted triangles and triangles marking the retrieved cloud base height (CBH) and cloud top height (CTH), respectively. The right column displays radiosonde profiles of relative humidity (RH, blue curve) and temperature (T, red curve); green horizontal bars denote cloud boundaries diagnosed via the humidity-gradient method of Xu et al. (2023). Each row (rows 1-6) corresponds to one validation case.

3. The spatial representativeness and scale matching should be discussed more carefully. Although the network is impressive, it is still a set of point measurements rather than an area-covering observing system. In addition, the MMCR observations are matched with ERA5 fields at 0.25° resolution, which may not represent local cloud environments well, especially over complex terrain or regions with strong surface heterogeneity. The authors may consider the sensitivity of key results to station distribution, sparse regions, complex terrain, and the point-to-grid matching method.

Response: We sincerely thank the Reviewer for this careful and constructive comment. We fully acknowledge that the 80 MMCR stations are point measurements rather than an area-covering observing system, and that matching them with 0.25° ERA5 fields may introduce scale mismatches, particularly over complex terrain and heterogeneous surfaces.

To address this concern, we have made two revisions:

(1) Sensitivity test with higher-resolution reanalysis

We repeated the key correlation analyses using ERA5-Land (0.1° × 0.1°, ~9 km), which better resolves near-surface heterogeneity. The comparison, now included in the Supplementary Materials (Figs. S5), shows that the correlation signs, spatial patterns, and magnitudes for CVS metrics against near-surface thermodynamic variables are highly consistent between ERA5 and ERA5-Land. This confirms that our core results are not sensitive to the specific grid resolution or to the point-to-grid scale mismatch.

We retained ERA5 as the primary dataset because our analysis requires atmospheric profiles (atmospheric temperature at the 700 hPa level ($T_{700\text{hPa}}$) and at the 500 hPa level ($T_{500\text{hPa}}$)) to compute lower-tropospheric stability (LTS_{surf}), which ERA5-Land does not provide. Using a single, physically consistent dataset for both surface and pressure-level variables is essential. The strong agreement between the two products in the sensitivity test further demonstrates that ERA5's 0.25° resolution is adequate for capturing the large-scale thermodynamic signals relevant to CVS.

(2) Explicit discussion of the limitation in the manuscript

We have added a paragraph in Section 2.2.3 that explicitly acknowledges the scale mismatch and presents the sensitivity test as a validation, as follows:

"*A spatial scale mismatch inevitably exists between the gridded ERA5 fields (~31 km) and the point-based MMCR observations, which may introduce uncertainties over complex terrain and regions with strong surface heterogeneity. To evaluate the sensitivity of our results to this mismatch, we repeated the key correlation analyses* *using ERA5-Land (0.1°× 0.1°, ~9 km), which better resolves near-surface variability. The comparison (Supplementary Figs. S5) shows that the correlation signs, spatial patterns, and magnitudes are highly consistent between the two products, confirming that our conclusions are not sensitive to the specific grid resolution. While some local-scale uncertainty is inherent in any point-to-grid comparison, the consistent spatial patterns across diverse climatic and topographic settings indicate that the identified relationships reflect robust large-scale physical mechanisms. The procedure for temporally aggregating the MMCR observations and matching them with ERA5 is described in Section 2.3.*"

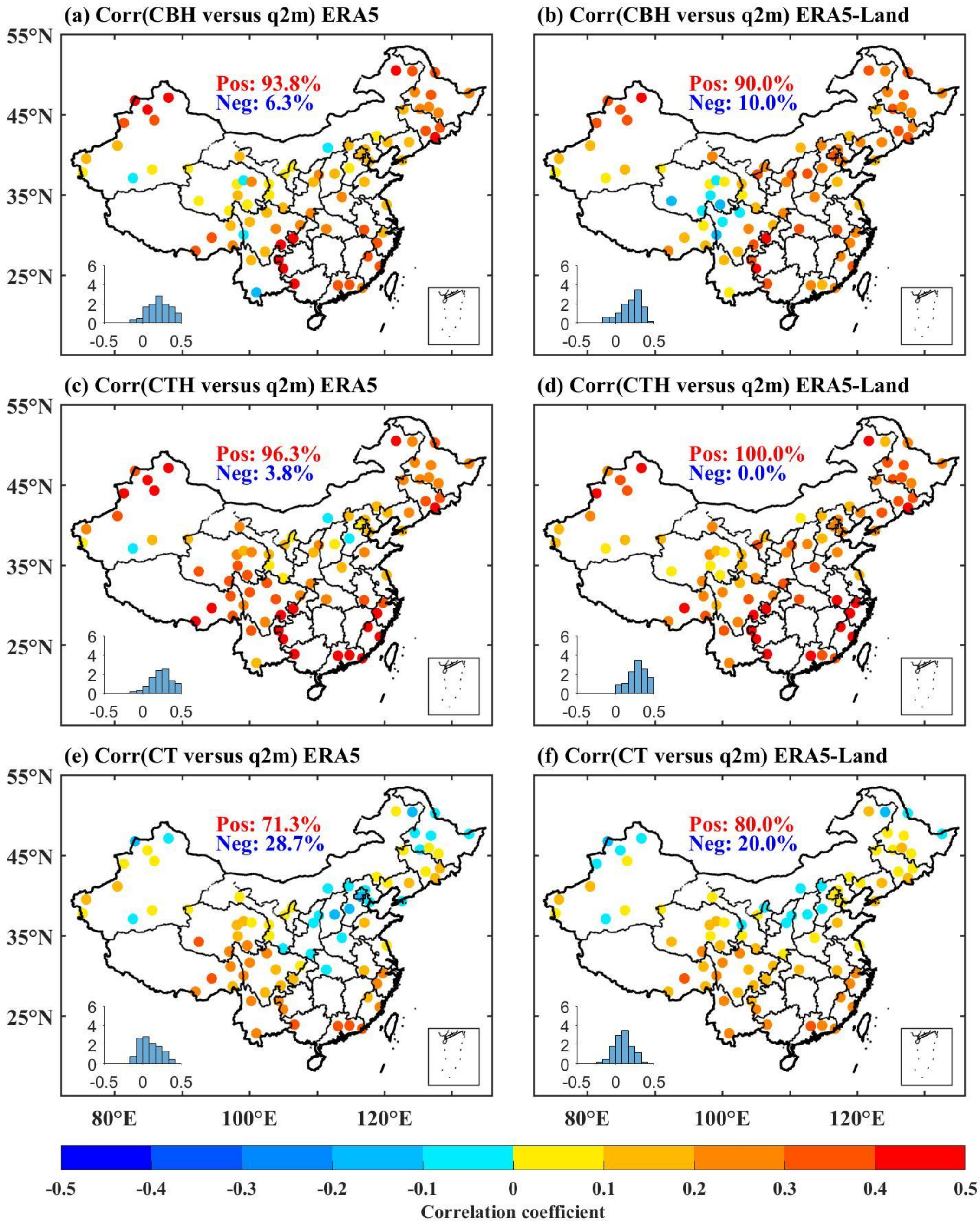

Figure S5. Comparison of the spatial correlations of CBH, CTH, and cloud thickness (CT) with 2m specific humidity (q2m) from ERA5 and ERA5-land across China (2024). All atmospheric variables were spatially and temporally matched with the MMCR CBH observational data to ensure the reliability of the correlation analysis. In each panel, the probability distribution of the correlation coefficient is illustrated by a histogram, and the abbreviations "Pos" and "Neg" denote the percentages of statistically significant positive and negative correlation coefficients across the entire study domain, respectively.

4.The physical attribution is still mainly based on correlation. The reported relationships between q850, LTS, WS700, and cloud properties are plausible, but the current analysis does not fully separate the effects of season, region, cloud type, and large-scale weather regime. For example, the positive relationship between q850 and CBH may partly reflect the co-occurrence of high humidity, deeper boundary layers, and convective regimes in summer, rather than a direct moisture effect on cloud base.

Response: We sincerely thank the reviewer for this constructive comment. We fully agree that correlations alone cannot definitively establish causality and that the effects of season, cloud type, and large-scale regime should be isolated to the extent possible. In the revised manuscript, we have taken the following steps to address this concern:

(1) Separation of seasonal and cloud-type effects

We have performed seasonal composite analyses for the correlations between all three cloud metrics (CBH, CTH, CT) and each atmospheric variable (q_{2m}, LTS_{surf}, VWS). The proportions of stations showing positive/negative correlations in each season are now reported and discussed (see Section 3.5; supplementary Figs. S6–S8). These results reveal distinct seasonal modulations. For instance, the positive CBH–q_{2m} correlation is strongest in summer (85% of stations) and weakest in spring (64.6%), supporting the interpretation that this relationship is largely governed by the seasonal prevalence of deep convective boundary layers rather than by a direct, season-independent moisture effect on cloud base. Similar seasonal contrasts are documented and discussed for LTS_{surf} and VWS, where the dominant cloud type (convective vs. stratiform) in each season is shown to condition the sign and strength of the correlations.

(2) Separation of thermodynamic and dynamic controls via joint dependence analysis

To further disentangle the intertwined effects of moisture, stability, and shear, we have introduced paired-variable joint dependence analyses (Figs. 9, 11, 13). These analyses explicitly demonstrate the conditional nature of the controls. For example, the positive effect of q_{2m} on CBH is only operative under low-LTS_{surf} (unstable) conditions and is largely suppressed under stable stratification. This directly addresses the Reviewer's concern by showing that the apparent positive q_{2m}–CBH correlation does not simply reflect the co-occurrence of high humidity and deep boundary layers, but rather a conditional coupling that requires convective instability.

(3) Regional information

The spatial maps of the correlations (Figs. 8, 10, 12) are retained and discussed, highlighting regional contrasts (e.g., distinct behaviour over the Tibetan Plateau, northwestern China, and the southeastern coastal regions). This preserves the geographical perspective within a nationally scaled analysis.

(4) Acknowledged limitations and future work

We acknowledge that our attribution remains correlation-based and that a formal separation by synoptic weather regimes—as the Reviewer rightly suggests—would further strengthen the mechanistic understanding. In the revised text, we have noted that while seasonal stratification captures the dominant large-scale regime shifts (e.g., monsoon vs. winter monsoon), a dedicated weather-regime analysis is beyond the scope of the current study. We have added a statement at the end of Section 4 acknowledging that while seasonal stratification captures the dominant large-scale regime shifts, a dedicated weather-regime analysis is beyond the scope of this study and is warranted in future work, as follows:

"*…. Additionally, while the seasonal stratification in this study captures the dominant large-scale regime shifts (e.g., monsoon), a dedicated analysis using objective weather-typing techniques would further isolate the effects of synoptic weather regimes on CVS, which is beyond the scope of the current study.*"

We believe these additions significantly strengthen the physical attribution and directly address the reviewer's concern. The seasonal and joint-dependence analyses demonstrate that the reported relationships are not mere statistical artifacts of seasonal aggregation, but reflect genuine, regime-dependent physical couplings.

For the sake of brevity, here we only show the revised text of the CBH case, as follows,

"*3.5.1 Impact of atmospheric thermodynamic factors on CBH*

Figure 8 illustrates the spatial distributions of annual mean correlation coefficients between CBH and three atmospheric variables. Positive correlations between CBH and q_{2m} are found at 93.8% of all observation stations (Fig. 8a), while only 6.3% of stations show negative correlations. This widespread positive relationship indicates that climatologically moister low-level environments are generally accompanied by higher cloud bases. Notably, this relationship does not imply that increased surface moisture directly lifts the LCL. Instead, it reflects the co-variability of low-level moisture and convective instability. Seasonal composite analyses further verify that this positive relationship between CBH and q_{2m} is most pronounced in summer (85% of stations), and weakest in spring (64.6%), with winter

(74.7%) and autumn (66.3%) falling in between (Fig. S6 a-d). Such seasonal contrast demonstrates that the CBH is governed by boundary layer depth and convective regimes, instead of a straightforward moisture-driven effect on cloud base height. Under moist and unstable conditions, a more deeply developed PBL and stronger thermally driven updrafts act to elevate cloud bases, particularly for cumulus and convective cloud systems (Betts, 2004; Zhang and Klein, 2013). This relationship is statistically robust and spatially consistent across most regions, particularly over southeast China, where moist convection dominates cloud vertical development. The sparse negative correlations (6.3%) are likely governed by persistent large-scale subsidence, which decouples local moisture fluctuations from cloud formation (Wood, 2012; Myers and Norris, 2013).

In contrast, CBH exhibits predominantly negative correlations with LTS_{surf} *across 97.5% of stations (Fig. 8b). The strong negative correlations are concentrated over the southeastern coastal regions of China. Higher* LTS_{surf} *indicates stronger lower-tropospheric stratification, which suppresses boundary-layer growth and favours shallow stratiform clouds with lower cloud bases (Klein and Hartmann, 1993; Wood and Bretherton, 2006). Conversely, reduced* LTS_{surf} *enhances instability, facilitating more intense turbulent mixing in the boundary layer, and promoting the development of convective clouds with higher cloud bases (Slingo, 1987). Seasonal composite analyses further verify that this negative relationship is most widespread in autumn (80.0% of stations) and summer (73.8%), and relatively less so in winter (63.3%) and spring (62.0%) (Fig. S6 e-f). This seasonality indicates that the CBH–*LTS_{surf} *coupling is modulated by the prevailing convective and boundary-layer regimes. The more consistent negative correlations in summer and autumn align with the dominance of deep convection and stable stratiform conditions (Zhang and Klein, 2013; Guo et al., 2016), respectively, whereas the weaker connection in spring and winter suggests that synoptic transients may at times override the local stability control (Taszarek et al., 2019). This seasonal differentiation confirms that, while* LTS_{surf} *exerts a primary thermodynamic control on CBH, its influence is conditioned by the seasonal evolution of boundary layer and cloud regimes (Zhang and Klein, 2013).*

At the national scale, CBH exhibits a predominantly negative correlation with VWS across 77.8% of stations (Fig. 8c). This widespread negative correlation indicates that stronger vertical wind shear is generally associated with lower cloud bases. Physically, enhanced VWS promotes the entrainment of drier environmental air into the cloud layer, which intensifies droplet evaporation, reduces buoyancy, and suppresses deep convective development, lowering effective cloud bases (Weisman and Rotunno, 2000). The sparse positive correlations (22.2%) likely reflect localized regimes where moderate shear organizes convection and helps sustain updrafts, or where shear-induced low-level convergence promotes cloud formation under specific *instability conditions (Houze, 2018). Seasonal composite analyses confirm the robustness of this negative relationship, with the proportion of stations showing negative correlations ranging from 56.5% in summer to 70.0% in winter (Fig. S6 i-l). This seasonal consistency, albeit weaker than that observed for thermodynamic factors (q_{2m} and LTS_{surf}), reinforces the interpretation that VWS plays a secondary modulating role in controlling CBH, conditioned by the prevailing convective regime.*

To further explore the joint constraints of atmospheric factors on CBH, we analyze the paired dependence of CBH on q_{2m}, LTS_{surf}, and VWS (Fig. 9). For the q_{2m}-LTS_{surf} combination (Fig. 9a), CBH generally increases with increasing q_{2m}, while the magnitude of this sensitivity is strongly modulated by atmospheric stability. Under low LTS_{surf} (unstable) conditions, the highest CBH values occur in moisture-abundant environments, consistent with deep boundary layers and active convective cloud development (Zhang and Klein, 2013). In contrast, under high LTS_{surf} (stable) conditions, CBH remains consistently low across nearly the entire moisture range, suggesting that strong lower-tropospheric stratification dominates the cloud base variation, confining cloud development to low-base stratiform clouds regardless of moisture availability (Klein and Hartmann, 1993; Wood and Bretherton, 2006).

The LTS_{surf}-VWS relationship (Fig. 9b) further illustrates this conditional modulation effect. In low LTS_{surf} environments, CBH tends to increase with increasing wind shear, consistent with the role of wind shear in organizing convection and modulating inflow structure under unstable conditions (Weisman and Rotunno, 2000). Under high LTS_{surf} environments, CBH remains uniformly low and shows weak sensitivity to shear, reinforcing the conclusion that stability exerts the primary constraint on cloud-base variability.

For the q_{2m}-VWS pairing (Fig. 9c), CBH increases primarily with q_{2m}, while wind shear plays a secondary modulating role. The highest CBH values occur when abundant low-level moisture coincides with weak-to-moderate wind shear, indicating that abundant low-level moisture acts as the primary driver for elevated cloud bases, while weak shear does not exert the suppressing effect typically associated with strong wind shear. This is consistent with the national-scale negative correlation between CBH and VWS shown in Fig. 8c, where strong shear environments tend to suppress cloud-base height.

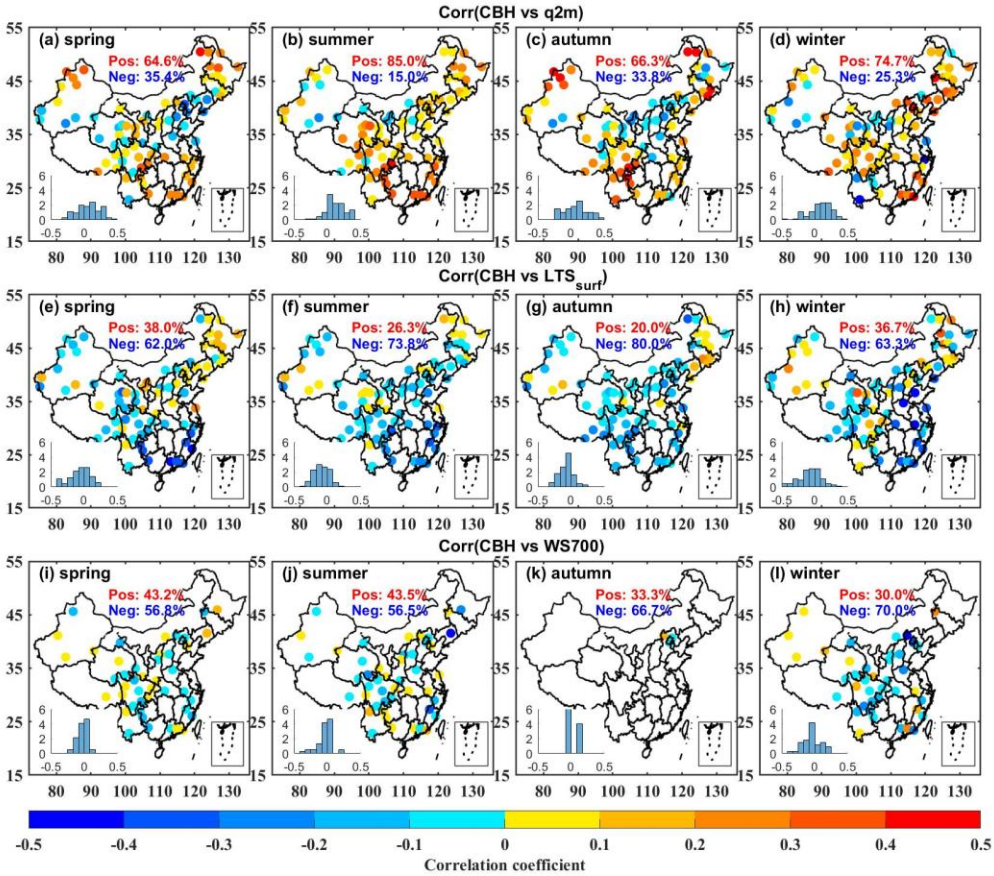

Figure S6*. Seasonal mean spatial correlations of CBH with (a-d) q_{2m}, (e-h) lower-tropospheric stability (LTS_{surf}), and (i-l) vertical wind shear (VWS) across China in 2024. All atmospheric variables were spatially and temporally matched with the MMCR CBH observations. In each panel, the histogram shows the probability distribution of the correlation coefficients, and the labels "Pos" and "Neg" indicate the percentages of stations with statistically significant positive and negative correlations, respectively.*"

5.CT should be treated carefully, since it is defined as the distance between the highest cloud top and lowest cloud base and may include clear gaps in multilayer cases. Clarifying this definition would make the interpretation of CT correlations more reliable.

Response: We have explicitly clarified this definition in the revised introduction sections (Lines 125-127), as follows:

"CT represents the total cloud thickness, defined as the difference between the highest CTH and lowest CBH across all detected layers. For multi-layer cloud conditions, this definition includes the clear-sky gaps between individual cloud layers."

6. The use of fixed pressure-level environmental variables needs caution, especially over the Plateau area. The manuscript uses q850 and an LTS definition based on 700 hPa and 1000 hPa, but these pressure levels may be below ground or not physically representative at high-elevation sites.

Response: We thank the reviewer for this critical comment. We fully agree that adopting fixed pressure-level variables (i.e., 850hPa specific humidity (q_{850}) and the traditional lower tropospheric stability (LTS = $\theta_{700hPa} - \theta_{1000hPa}$)) is inappropriate over the Tibetan Plateau. In the revised manuscript, we have replaced these with elevation-dependent formulations that maintain physical representativeness across all terrain heights. The specific modifications are as follows:

Low-level moisture:

The q_{850} has been replaced with 2 m specific humidity (q_{2m}), which is calculated from the ERA5 2 m dewpoint temperature ($T_{d,2m}$) and surface pressure (p_{surf}) using standard psychrometric formulas. Because q_{2m} is defined at 2m above the surface, it inherently follows the topography, making it a physically consistent measure of low-level moisture across all terrain heights, including the Tibetan Plateau.

Lower-tropospheric stability and vertical wind shear:

For both LTS and VWS, we adopt a unified terrain-following criterion based on surface elevation rather than using a single fixed pressure level:

For stations with surface elevation < 3 km (covering most of eastern and central China), we use the 700 hPa level to calculate LTS ($\theta_{700hPa} - \theta_{surf}$) and WS700. This is consistent with classical definitions for lowland regions.

For stations with surface elevation ≥ 3 km (typical of the Tibetan Plateau), we raise the reference pressure level to 500 hPa to calculate LTS ($\theta_{500hPa} - \theta_{surf}$) and WS500.

This elevation-dependent approach ensures that the vertical distance between the surface and the reference pressure level is roughly comparable (~2–3 km) across all stations (lowlands: surface→700 hPa; Plateau: surface→500 hPa). This prevents the 700 hPa level—which lies within the highly variable and friction-influenced near-surface layer over the Plateau—from artificially dominating the stability and shear calculations, thereby providing a more robust and physically consistent quantification of the large-scale thermodynamic and dynamical controls on cloud vertical structure.

Reanalysis and robustness verification:

All correlation and joint-dependence analyses presented in Sections 3.5 have been repeated using the updated variables. The revised results, including the spatial distributions, correlation signs, and statistical significance for the relationships between CBH, CTH, CT and moisture, stability as well as wind shear are shown in Figures 8-13. We have added detailed descriptions of the above modifications in Section 2.2.3 (ERA5 reanalysis) and included a brief clarification is Section 3.5.

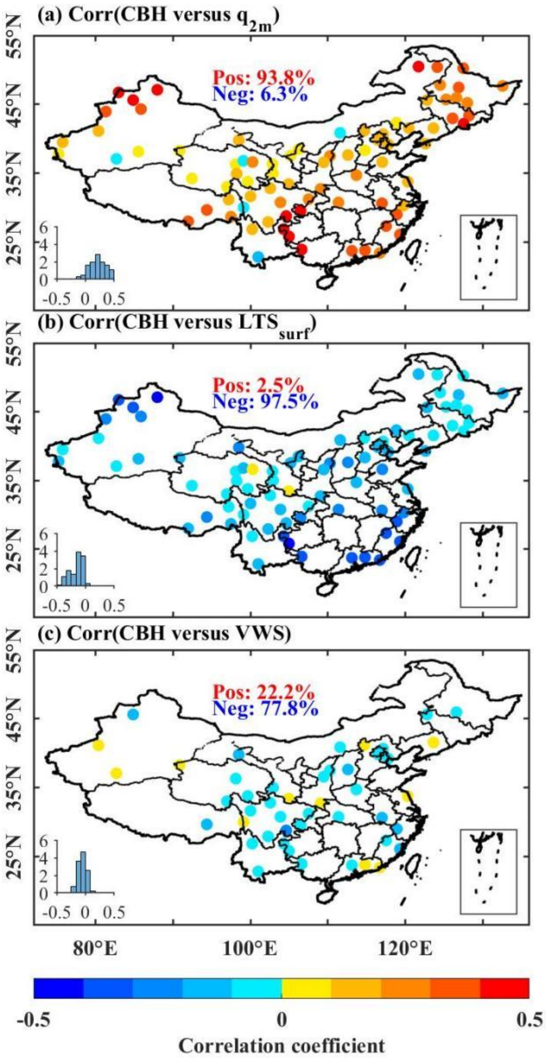

***Figure 8**. Spatial distributions of correlation coefficients of CBH with lower-tropospheric stability (LTS), 2 m specific humidity (q_{2m}), and vertical wind shear (VWS) across China (2024). Here, LTS_{surf} is defined as the difference between potential temperature at the reference pressure level (700 hPa for low-elevation sites and 500 hPa for high-elevation sites) and surface potential temperature. The VWS is calculated at the same reference levels following the elevation-dependent scheme described in Section 2.2.3. All atmospheric variables were spatially and temporally matched with the MMCR CBH observational data to ensure the reliability of the correlation analysis. In each panel, the probability distribution of the correlation coefficient is illustrated by a histogram, and the abbreviations "Pos" and "Neg" denote the percentages of statistically significant positive and negative correlation coefficients across the entire study domain, respectively.*

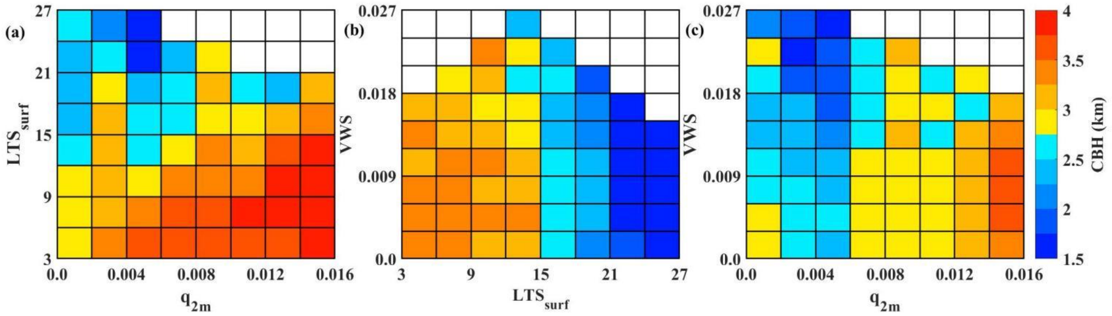

Figure 9. *Bivariate regulation of CBH by thermodynamic and dynamical factors across China in 2024, based on observations from 80 MMCR stations. Each panel illustrates the response of CBH to the combined modulating effects of a specific pair of key atmospheric factors: (a) q_{2m} and LTS$_{surf}$, (b) LTS$_{surf}$ and VWS, and (c) q_{2m} and VWS. All ERA5 reanalysis variables were spatially and temporally collocated with MMCR observations to ensure the validity and reliability of this bivariate joint dependence analysis.*

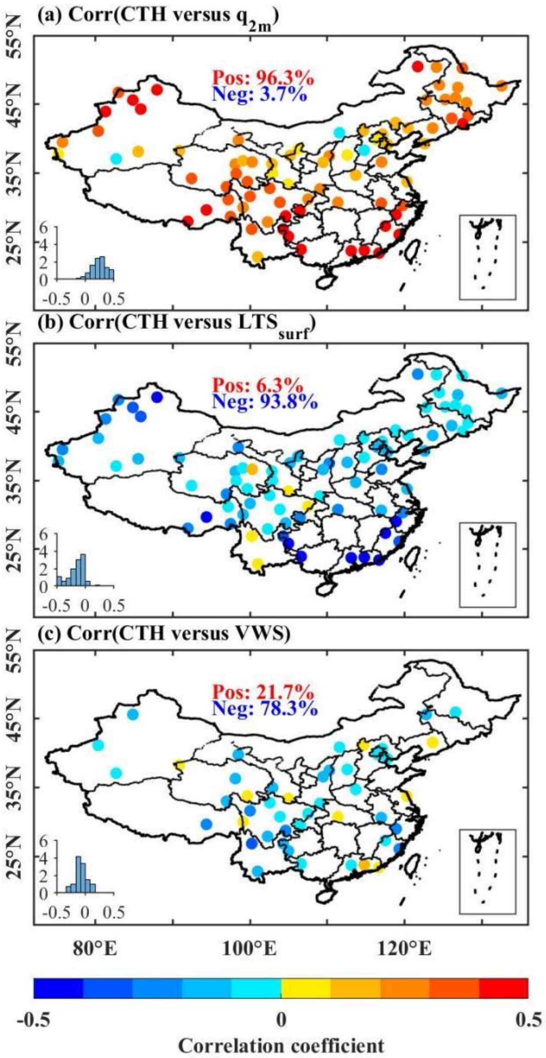

Figure 10*. Similar as Figure 8, but for the CTH.*

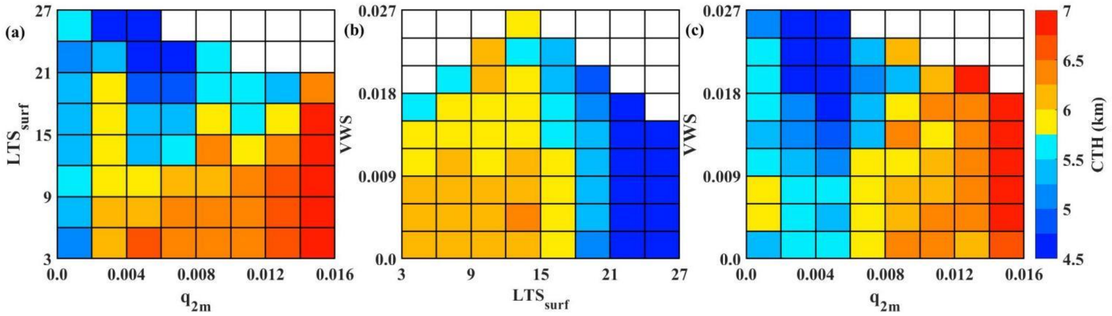

Figure 11. *Similar as Figure 9, but for CTH.*

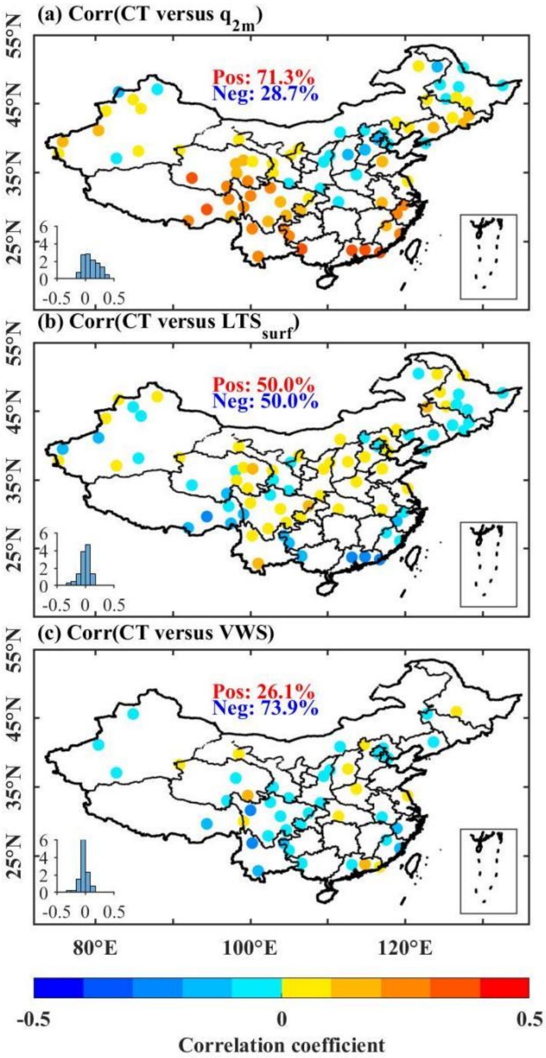

Figure 10*. Similar as Figure 8, but for CT.*

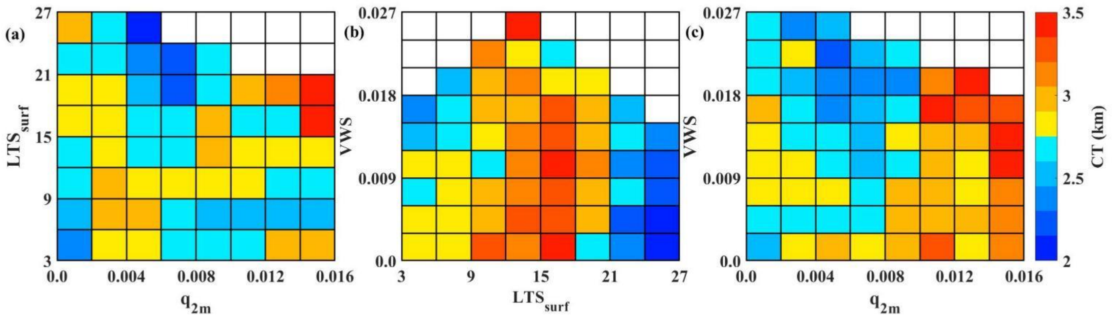

Figure 13. *Similar as Figure 9, but for CT.*

The sentences "*In this study, we use ERA5 data for 2024 to examine the impacts of LTS and specific humidity on CVS. For this purpose, hourly temperature at 1000 hPa and 700 hPa, and specific humidity at 850 hPa (q_{850}) are extracted for all 80 selected MMCR stations.*" in the section 2.2.3 was revised as follow:

"*In this study, we use ERA5 data for 2024 to examine the impacts of LTS and specific humidity on CVS. For this purpose, hourly 2 m air temperature (T_{2m}), atmospheric temperature at the 700 hPa level (T_{700hPa}) and at the 500 hPa level (T_{500hPa}), 2 m dewpoint temperature ($T_{d,2m}$), and surface pressure (p_{sfc}) are extracted for all 80 selected MMCR stations. The 2 m specific humidity (q_{2m}) is calculated from $T_{d,2m}$ and p_{surf} using standard psychrometric formulas. Because q_{2m} is defined at 2 m above the surface, it inherently follows the topography, making it a physically consistent measure of low-level moisture across all terrain heights, including the Tibetan Plateau.*"

The updated metrics also improve the reliability of analyses regarding thermodynamic controls on cloud vertical structure across diverse terrains, especially over the Tibetan Plateau.